9-1-2017

Characteristics of mesospheric gravity waves over Antarctica observed by ANGWIN (Antarctic Gravity Wave Instrument Network) imagers using 3-D spectral analyses

Takashi S. Matsuda
Graduate University for Advanced Studies, Tachikawa, Japan

Takuji Nakamura
Graduate University for Advanced Studies, Tachikawa, Japan

Mitsumu K. Ejiri
Graduate University for Advanced Studies, Tachikawa, Japan

Masaki Tsutsumi
Graduate University for Advanced Studies, Tachikawa, Japan

Yoshihiro Tomikawa
Graduate University for Advanced Studies, Tachikawa, Japan

Follow this and additional works at: https://digitalcommons.usu.edu/ail_pubs

Part of the Atmospheric Sciences Commons

See next page for additional authors

Recommended Citation
Matsuda T.S., T. Nakamura, M.K. Ejiri, M. Tsutsumi, Y. Tomikawa, M.J. Taylor, Y. Zhao, P.-D. Pautet, D.J. Murphy, and T. Moffat-Griffin, Characteristics of mesospheric gravity waves over Antarctica observed by ANGWIN (Antarctic Gravity Wave Instrument Network) imagers using 3-D spectral analyses, J. Geophys. Res., DOI: 10.1002/2016JD026217, 2017

AGU PUBLICATIONS

JGR

Journal of Geophysical Research: Atmospheres

RESEARCH ARTICLE
10.1002/2016JD026217

Special Section:
Atmospheric Gravity Wave Science in the Polar Regions and First Results from ANGWIN

Characteristics of mesospheric gravity waves over Antarctica observed by Antarctic Gravity Wave Instrument Network imagers using 3-D spectral analyses

Takashi S. Matsuda[1,2], Takuji Nakamura[1,2], Mitsumu K. Ejiri[1,2], Masaki Tsutsumi[1,2], Yoshihiro Tomikawa[1,2], Michael J. Taylor[3], Yucheng Zhao[3], P.-Dominique Pautet[3], Damian J. Murphy[4], and Tracy Moffat-Griffin[5]

[1]Graduate University for Advanced Studies, Tachikawa, Japan, [2]National Institute of Polar Research, Tachikawa, Japan, [3]Physics Department at Utah State University, Logan, Utah, USA, [4]Australian Antarctic Division, Kingston, Tasmania, Australia, [5]British Antarctic Survey, Cambridge, UK

Abstract We have obtained horizontal phase velocity distributions of the gravity waves around 90 km from four Antarctic airglow imagers, which belong to an international airglow imager/instrument network known as ANGWIN (Antarctic Gravity Wave Instrument Network). Results from the airglow imagers at Syowa (69°S, 40°E), Halley (76°S, 27°W), Davis (69°S, 78°E), and McMurdo (78°S, 167°E) were compared, using a new statistical analysis method based on 3-D Fourier transform (Matsuda et al., 2014) for the observation period between 7 April and 21 May 2013. Significant day-to-day and site-to-site differences were found. The averaged phase velocity spectrum during the observation period showed preferential westward direction at Syowa, McMurdo, and Halley, but no preferential direction at Davis. Gravity wave energy estimated by I'/I was ~5 times larger at Davis and Syowa than at McMurdo and Halley. We also compared the phase velocity spectrum at Syowa and Davis with the background wind field and found that the directionality only over Syowa could be explained by critical level filtering of the waves. This suggests that the eastward propagating gravity waves over Davis could have been generated above the polar night jet. Comparison of nighttime variations of the phase velocity spectra with background wind measurements suggested that the effect of critical level filtering could not explain the temporal variation of gravity wave directionality well, and other reasons such as variation of wave sources should be taken into account. Directionality was determined to be dependent on the gravity wave periods.

Key Points:
- Various variabilities of the mesospheric gravity waves are found for the first time by an airglow network observation in the Antarctic
- The phase velocity spectrum that indicated wind filtering effect of gravity waves is significant over Syowa, Halley, and McMurdo
- Over Davis, however, no preferential propagation direction is found, which could be because of secondary wave generation

Correspondence to:
T. S. Matsuda,
matsuda.takashi@nipr.ac.jp

Citation:
Matsuda, T. S., T. Nakamura, M. K. Ejiri, M. Tsutsumi, Y. Tomikawa, M. J. Taylor, Y. Zhao, P.-D. Pautet, D. J. Murphy, and T. Moffat-Griffin (2017), Characteristics of mesospheric gravity waves over Antarctica observed by Antarctic Gravity Wave Instrument Network imagers using 3-D spectral analyses, *J. Geophys. Res. Atmos.*, *122*, 8969–8981, doi:10.1002/2016JD026217.

Received 10 NOV 2016
Accepted 27 JUL 2017
Accepted article online 30 JUL 2017
Published online 1 SEP 2017

1. Introduction

Atmospheric gravity waves (AGWs) play an important role in the global atmospheric circulation through momentum transport and deposition from the lower atmosphere into the mesosphere and lower thermosphere, which accelerates the mean wind in the mesosphere [e.g., *Lindzen*, 1981; *Fritts and Alexander*, 2003]. Short-period ($<$ 1 h) small-scale AGWs are thought to mostly contribute to vertical transport of the momentum in the middle atmosphere [Vincent, 1984].

The airglow imaging technique, which measures the optical emissions of the airglow layers located around 85–100 km altitude, is very useful for investigating the horizontal structure of mesospheric AGWs (e.g., horizontal wavelength, observed period, observed phase speed, wave propagation direction, occurrence, and duration) [e.g., *Taylor et al.*, 1997; *Walterscheid et al.*, 1999; *Lu et al.*, 2015a]. Among these parameters, the phase velocity distribution (phase speed and propagation direction) is quite important in understanding the characteristics of AGW generation and propagation processes [e.g., *Lindzen*, 1981]. For a quarter of a century, statistical studies of the AGW phase velocity distribution observed by airglow imaging techniques have been performed primarily at middle [e.g., *Nakamura et al.*, 1999; *Walterscheid et al.*, 1999; *Hecht et al.*, 2001] and low latitudes [e.g., *Taylor et al.*, 1997; *Li et al.*, 2011]. Airglow observations in Antarctica have been difficult until recent years [e.g., *Espy et al.*, 2006; *Nielsen et al.*, 2009, 2012; *Bageston et al.*, 2009; *Suzuki et al.*, 2011; *Matsuda et al.*, 2014] due to auroral contamination and logistical difficulties. A quantitative comparison of phase velocity distributions at multiple observation sites has been done in the middle or low latitudes [*Ejiri et al.*, 2003; *Wrasse et al.*, 2006] but has not been conducted for the Antarctic. Comparison among the previous Antarctic observations is not easy because data analyses were performed primarily using manual identification methods where a person identified AGW events directly by viewing the

Table 1. Summary of the Four Airglow Imagers Used in This Study[a]

Station	Latitude, Longitude	mLat	Institution	Airglow	Sampling Interval	Exposure	Detector Size
Syowa (Japan)	69°S, 40°E	66°S	NIPR	Na (589.0, 589.6 nm)	1 min	45 s	512 × 512
Davis (Australia)	69°S, 78°E	77°S	Utah State University	OH (0.9–1.7 μm)	10 s	3 s	320 × 256
McMurdo (USA)	78°S, 167°E	81°S	Utah State University	OH (0.9–1.7 μm)	10 s	3 s	320 × 256
Halley (UK)	76°S, 27°W	67°S	Utah State University	OH (0.9–1.7 μm)	10 s	3 s	320 × 256

[a]Sampling intervals of Utah State University's three imagers at Davis, Halley, and McMurdo are converted to 1 min by averaging six images. We assume that Na altitude is 90 km and OH altitude is 87 km.

airglow imagery and then uses well-documented techniques [e.g., *Hapgood and Taylor*, 1982; *Garcia et al*., 1997] to derive the AGW parameters. These manual methods have two limitations: a possible bias caused by different event extraction criteria depending on the person performing the analysis and the long time required to analyze the large amount of image data such as the Antarctic Gravity Wave Instrument Network (ANGWIN).

In this study, we use a new spectral analysis method developed by *Matsuda et al*. [2014] in order to obtain power spectra of airglow intensity variation in the horizontal phase velocity domain from long time series of airglow images by using a three-dimensional (3-D) Fourier transform described in *Coble et al*. [1998]. This method is applied to airglow imaging data observed by ANGWIN, an international observation network involving several Antarctic stations which commenced coordinated operations in 2011, and aiming at investigating the AGWs over the Antarctic Continent. ANGWIN includes airglow imagers operated at Syowa (69°S, 40E°), Davis (69°S, 78°E), McMurdo (78°S, 167°E), Halley (76°S, 26°E), Rothera (68°S, 68°W), South Pole (90°S), and Comandante Ferraz (62°S, 58°W).

We will present and discuss the first geographical and day-to-day variability in phase velocity distributions observed by four ANGWIN imagers. The phase velocity distributions will be compared with background wind measurements in order to investigate the AGW generation and propagation process. Temporal variations during one night and frequency dependency of the phase velocity spectrum are also presented.

2. Observation and Analysis

We used data observed automatically by four imagers out of the ANGWIN network: a Na imager at Syowa and three nearly identical broadband IR imagers operated at Davis, Halley, and McMurdo as described in Table 1 and Figure 1. The Na imager at Syowa is equipped with a CCD camera (HAMAMATSU C-4880-72) with 512 × 512 pixels and a lens of a Fish-eye Nikkor (F1.4 and f = 6 mm) with a field of view of 180°. Details of the imaging system were described by *Taguchi et al*. [2004]. The Na airglow at 589.0 and 589.6 nm was observed in order to avoid auroral contamination, together with background sky images at 572.5 nm which were used to correct the Na airglow intensity for background brightness. It should be noted that this correction is not needed for OH airglow because the background sky intensity is weaker than OH airglow intensity. Exposure time and cadence of the Na airglow images were 45 s and 1 min, respectively. Every 15 min the background sky image was observed. For this period of the background observation, the Na image was interpolated using adjacent two images. The observation was performed during nighttime (the Sun is at least 12° below the horizon) without moonlight. The 3 IR imagers are fitted with a 320 × 256 pixel indium gallium arsenide (InGaAs) detector, sensitive from 0.9 to 1.7 μm where auroral contamination is smaller than in wavelengths (visible–800 nm) to which CCD detectors are sensitive. The InGaAs imagers observe several OH emission bands, especially the bright (3,1) and (4,2) bands (>100 kR), allowing us to use a short (~2.5 s) exposure time and a high acquisition cadence (1 image every 10 s). A Fujinon E185C046H-1 C-mount fisheye lens makes it possible to observe the whole sky at once. The system is automatically controlled by a Windows computer through the USB port. Data are acquired during the entire winter season, when the Sun is at least 8° below the horizon, and even in the presence of moonlight. For this initial study the period between 6 April and 21 May 2013 was selected for analyses from the simultaneous observation periods, by investigating clear-sky statistics at Syowa station. Then, we selected data sets of successive images without clouds or auroral contamination, lasting for more than 1 h, and created time windows for the analyses. Figures 2a–2d show a summary of the time windows for our analyses bounded by the observation time at each site. Figure 2e shows the periods of clear sky for all four stations. Each station had seven

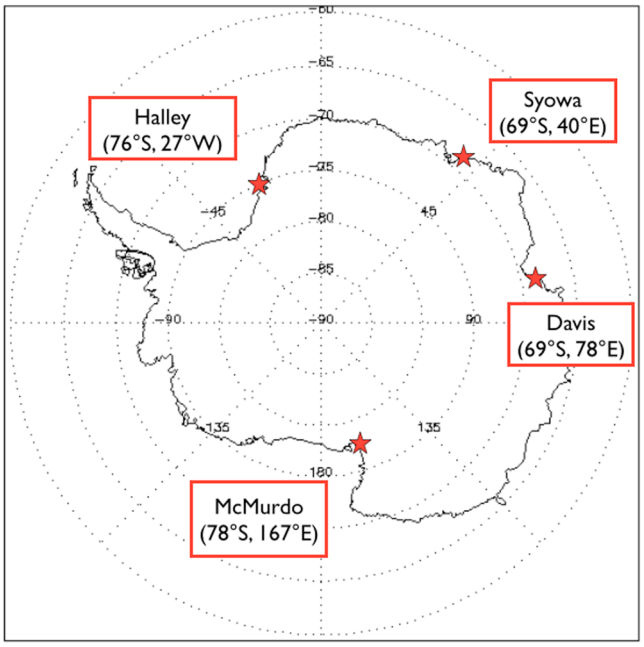

Figure 1. Locations of airglow imagers used in this study.

to nine analysis windows, and the total observation time for the analyses was 20–30 h. The details of the sky condition statistics are summarized in Table 2.

We applied a spectral analysis method developed by *Matsuda et al.* [2014] to the data observed at each of the four different stations to derive phase velocity spectra. This new technique can display the distribution of phase velocity and direction. Importantly, the intensity of the spectral component includes information on AGW amplitudes in the airglow images, the duration of the AGW event, and the spatial extent of the wave packet. Other advantages are that, compared with conventional manual analysis methods, it provides objective results with a shorter analysis time and it uses data spatially broader, longer in time, and wider in frequency.

In order to obtain phase velocity spectrum from the series of airglow images, we used several preprocesses, 3 Dimensional-Fast Fourier Transform (3d-FFT), coordinate conversion from the horizontal wave number domain into the horizontal phase velocity domain, and integration over the frequency. The preprocesses performed before the 3D-FFT are as follows: star removal, dark count removal, calculating relative airglow intensity perturbation, projection onto geographical coordinates, prewhitening, 2-D Hanning window, and zero padding. From the preprocessed images we obtained a 3-D spectrum as a function of frequency, zonal wave number, and meridional wave number, by using the 3-D discrete Fourier transformation [*Coble et al.*, 1998]. Next, the 3-D spectrum was converted to the phase velocity domain. Finally, the 3-D phase velocity spectrum was integrated in the frequency domain, and a 2-D phase velocity spectrum was calculated.

Although the basic spectral data analysis procedure is the same as described in *Matsuda et al.* [2014], several changes have been applied as follows. For the OH and Na airglow, images of I'/I, the airglow intensity perturbation normalized by the temporal mean of the airglow images, were projected onto the geographic coordinate system, assuming mean emission heights of 87 and 90 km, respectively. The projection onto the geographic coordinate system used an area of 256×256 km^2 with 1 km^2 pixel size, and then a 3-D array with a size of 1024 pixels × 1024 pixels × 240 images was created using a zero padding in order to improve the interval of the spectrum in wave number and frequency. It should be noted that the sampling interval of the Utah State University imagers was 10 s, and therefore six images were averaged in order to obtain 1 min interval images for compatibility with the Syowa measurement cadence. We extracted the spectral components with horizontal wavelengths of 10–100 km, periods of 8–60 min, and phase speeds of 0–150 m/s and regarded them as representing AGWs within these analysis ranges.

3. Results

3.1. Station-to-Station and Day-to-Day Variations

Vector directionality is important in the discussion of sources and vertical propagations of AGWs (e.g., critical level filtering by background winds [e.g., *Taylor et al.*, 1993]). The word, "directionality," is often used to express preferential direction, but, in this article, we treat the term "directionality" as dependency on both the wave propagation direction and its phase speed, which are displayed by the phase velocity spectrum. Although there are previous studies of day-to-day variation of AGW activity in the Antarctic [e.g., *Espy et al.*, 2004], day-to-day variation of AGW's directionality in the Antarctic has not been studied. Here we will show the variation between 10 and 11 April at Davis and McMurdo. Figures 3a and 3b show examples of

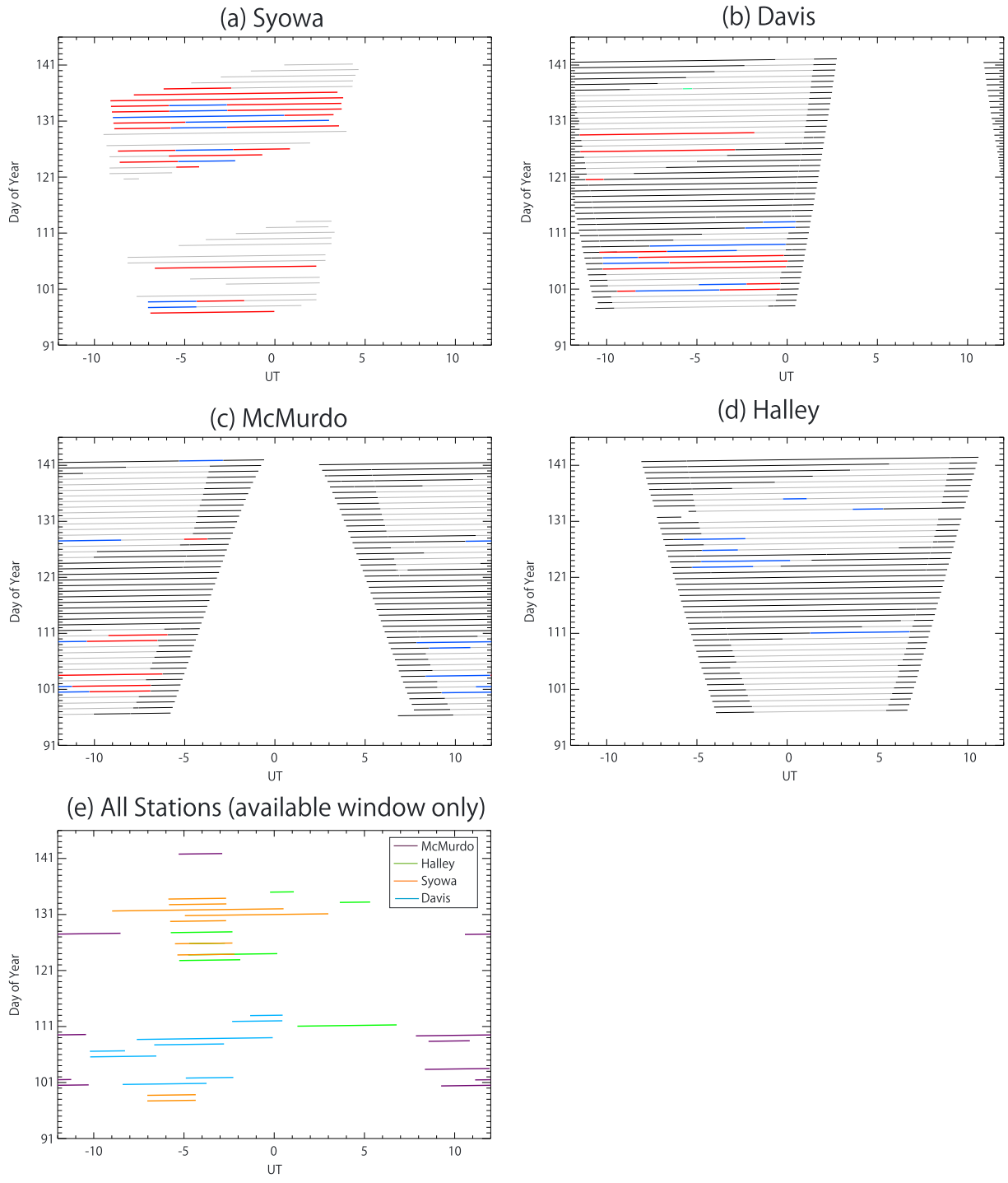

Figure 2. (a–d) Observation time of imagers at each ANGWIN site used in this study. The vertical axis is the day of the year in 2013. The color shows the sky condition. Blue, red, and gray represent clear sky, auroral contamination, and cloudy, respectively. Thick black lines show twilight or moonlight. (e) Summary of time of clear-sky imagers at the four stations. Different colors show observation sites. It should be noted that the green line of Halley at 1917–2116 UT on 5 May is not visible because the line is covered with the line of Syowa.

phase velocity spectral results at Davis as observed during intervals at 15:36–20:15 UT on 10 April and at 19:06–21:44 UT on 11 April 2013, respectively. On 10 April (Figure 3a) the spectral power in phase speeds below 60 m/s was stronger in the westward direction (150–320° clockwise from the north) and weaker in the northward direction (320–10°). However, for spectral components with phase speeds faster than

Table 2. Sky Condition Statistics at the Four Stations for 6 April to 21 May 2013

Station	Cloud (h)	Aurora (h)	Clear Sky (h)
Syowa	151.8	79.8	32.3
Davis	252.2	62.0	21.3
McMurdo	271.8	22	22.6
Halley	285.5	0	22.2

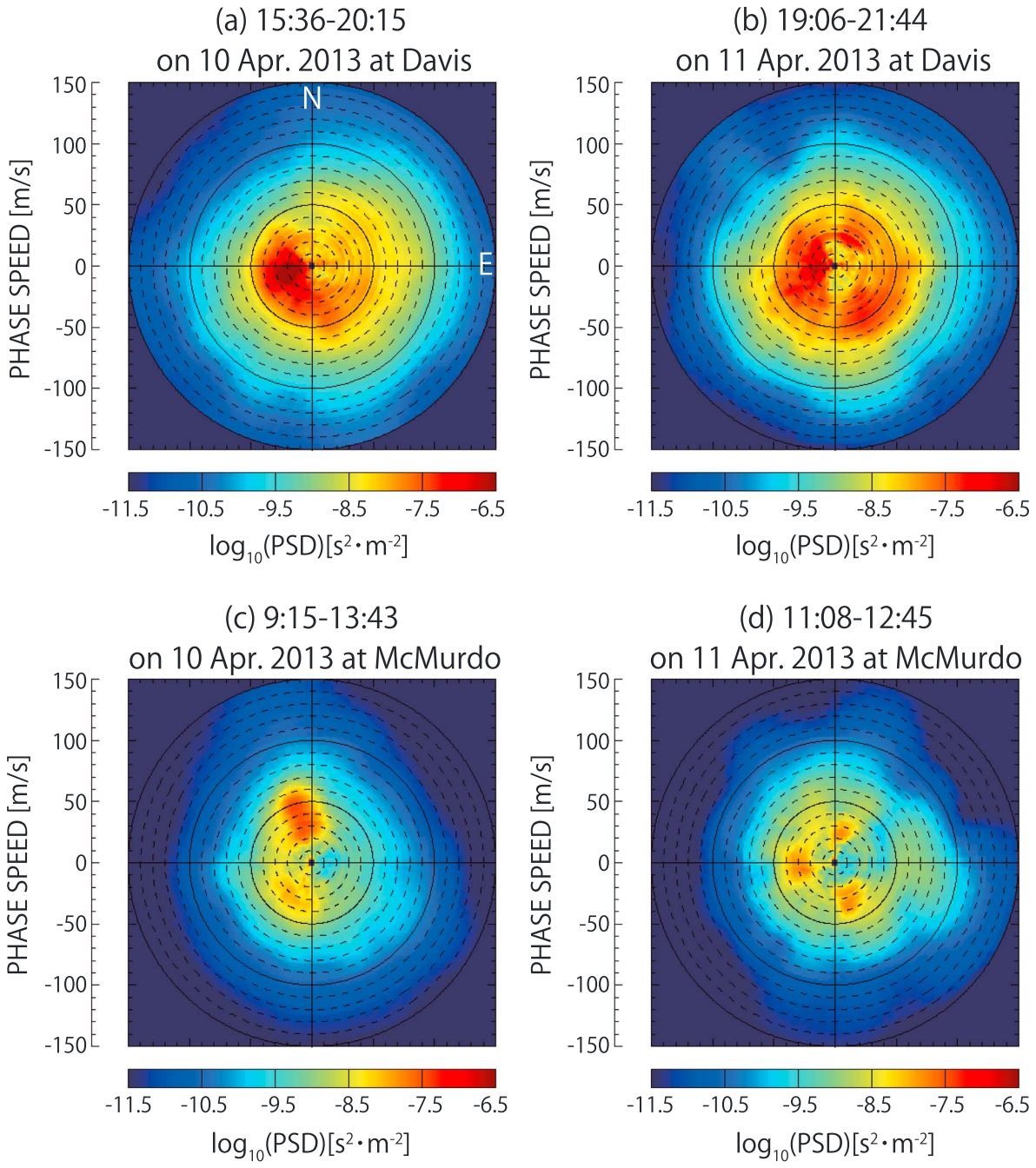

Figure 3. Phase velocity spectra on two consecutive nights, 10 and 11 April 2013 at (a and b) Davis and (c and d) McMurdo. Spectra on (a and c) 10 and (b and d) 11 April.

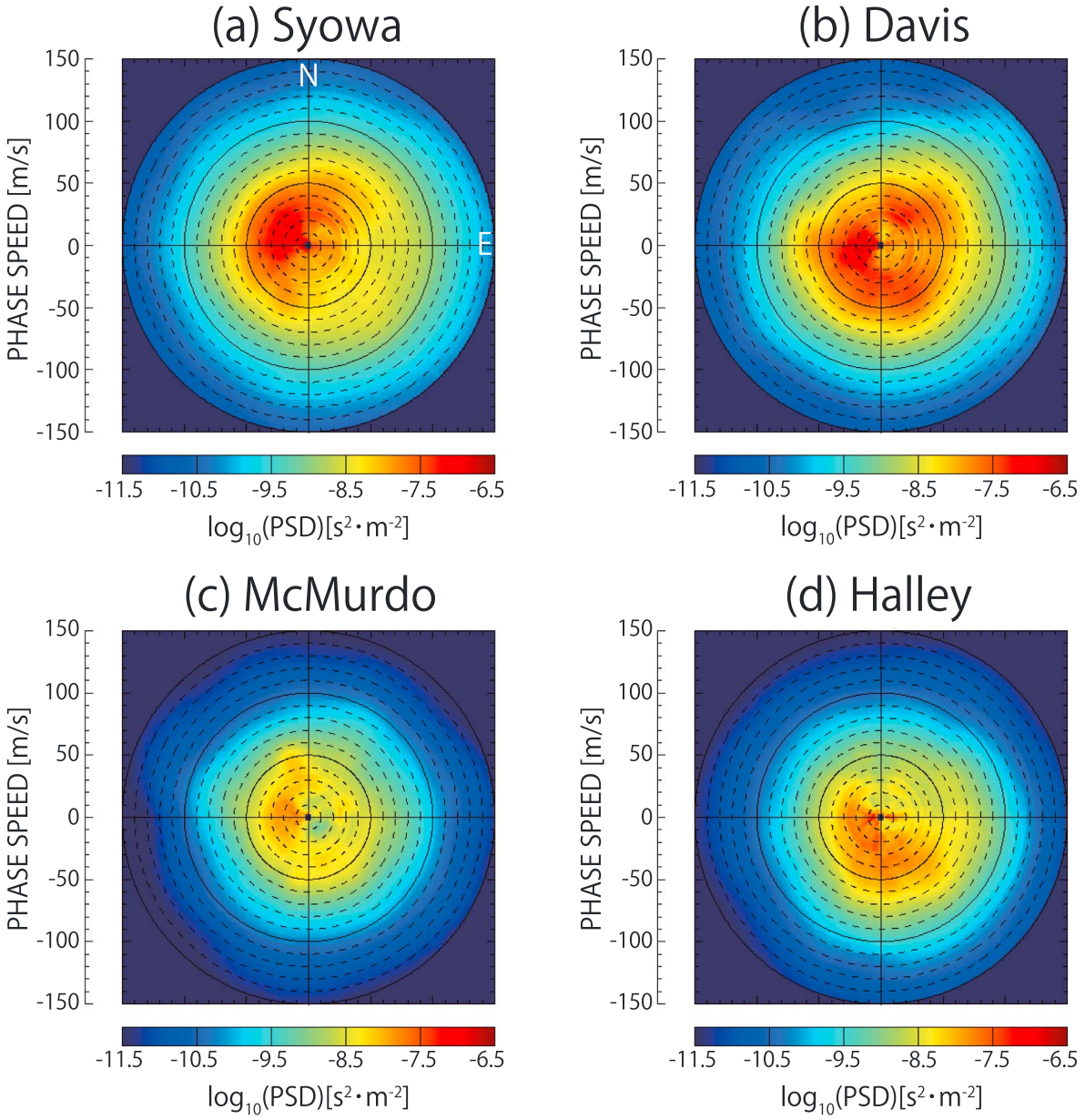

Figure 4. Phase velocity spectra averaged for the clear-sky nights between 6 April 2013 and 21 May 2013 observed at (a) Syowa, (b) Davis, (c) McMurdo, and (d) Halley.

60 m/s the spectral power was larger in the eastward direction (30–180°) and weaker in the westward direction (180–360°). On the next day, 11 April (Figure 3b), the spectrum was more uniform in azimuth for phase speeds slower than 70 m/s. Enhancements in the southeastward direction (80–180°) and in the westward direction (190–350°) were also observed with phase speeds 20–70 m/s and $<$50 m/s, respectively.

Figures 3c and 3d show the wave spectra for the same 2 day interval as obtained at McMurdo from 9:15 to 13:43 UT on 10 April 2013 and 11:08 to 12:45 UT on 11 April 2013, respectively. On 10 April (Figure 3c) the spectrum exhibited two peaks: one (strong) with phase speeds of 20–60 m/s at 320–10° in azimuth and the other (weaker) with phase speeds of 10–40 m/s at 180–230° in azimuth. On the next day, the wave spectrum (Figure 3d) exhibited three distinct peaks all in the same phase speed range 20–40 m/s at 0–30°, 140–180°, and 240–300° in azimuth (i.e., almost north, south, and west). Regions between these azimuth ranges also indicate faster waves with phase speeds 50–100 m/s, and region propagating mainly eastward is also noticeable.

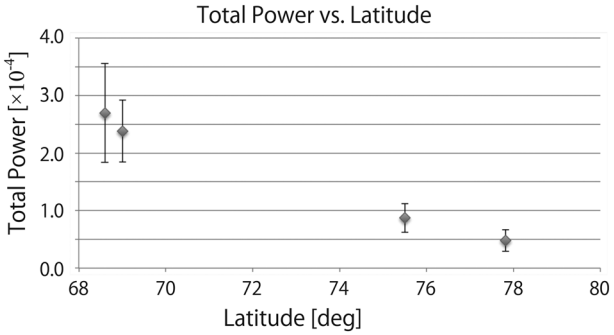

Figure 5. Total power of the monthly spectra which corresponds to variance of relative intensity variations, I′/I, plotted as a function of latitude. The error bar shows confidence interval of the averaged spectra.

These four spectra in Figure 3 demonstrate the strong day-to-day variations in the wave directionality between 10 and 11 April at Davis and McMurdo, and as well as difference in the directionality between the two stations on the same day. This suggests that the directionality of AGW over the Antarctic is highly variable in time and space.

In Figure 4 we compare average phase velocity spectra observed from 6 April to 21 May in 2013. The spectrum at Syowa (Figure 4a), averaged over the nine nights, showed an enhanced region in the westward direction (180–80°) for phase speeds <60 m/s, whereas an enhancement in the eastward direction was found for phase speeds faster than 70 m/s. This directionality is very similar to that previously reported for Syowa Station in 2011 [*Matsuda et al*., 2014, Figure 5b].

The spectrum at Davis (Figure 4b), averaged over the eight nights, was more uniform in phase speeds slower than 50 m/s as compared with the other spectra in Figure 4.

At McMurdo the averaged spectrum was obtained for the seven nights of the observations (Figure 4c). A weak peak in the northward direction (330–360°) with phase speeds of 20–50 m/s was found, which was mainly due to the AGW with strong power propagating in the northward direction on 10 April 2013, as shown in Figure 3c. Another enhancement can also be seen in phase speeds <40 m/s at 210–330° in azimuth. The AGW (northward) on 10 April had a large spectral power and greatly contributed to the averaged spectrum. An AGW with large spectral power carries large momentum, because measured AGW power is proportional to duration, spatial extent, and the square of wave amplitude. Thus, an AGW with large momentum greatly affects the averaged spectrum. The case on 10 April is a good example of the ability of spectrum analysis to express AGW energy as spectral power.

The averaged spectrum at Halley derived from the seven nights (Figure 4d) had a southward broad enhancement for phase speeds <70 m/s at 110–220° in azimuth. Westward enhancement at 210–330° in azimuth and with speeds <30 m/s was also recognized.

Among the four averaged spectra, the more uniform directionality observed at Davis was exceptional. The other three stations exhibited preferential propagation primarily in the westward direction and generally lacked waves in the southeastward direction at Syowa, the eastward direction at McMurdo, and the northeastward direction at Halley (possibly caused by critical level filtering by background wind). This topic will be discussed in more detail in sections 3.2 and 3.3.

Next, we examined averaged gravity wave energy by integrating the power spectra shown in Figure 4 for all the phase speeds between 0 and 150 m/s. This integrated value corresponds to the variance of I′/I and represents gravity wave energy because I′/I is proportional to relative temperature perturbation by AGW (T′/T) [e.g., *Gardner et al*., 1999; *Espy et al*., 2004]. The resultant "wave power" at each station is plotted as a function of latitude in Figure 5. It is clear that the spectral power was smaller at higher latitudes. The spectral power at Davis was 5–6 times larger than that at McMurdo, which is located 9° farther south than Davis. *Yamashita et al*. [2009] compared potential energy of gravity waves in the stratosphere (30–45 km altitude) observed by lidars at Rothera (67.5°S) and South Pole (90°S) (their Figure 4c). The potential energy in May at Rothera was 5 times larger than that at the South Pole, with the two stations located 22.5° in latitude apart. It is interesting to note that the similar factor of the energy difference (~5 times) was achieved by only 9° difference in latitude in the mesopause region. The significant decrease of the wave energy at the mesopause heights between Davis and McMurdo could be due to the fact that the AGWs analyzed in our airglow observations exhibited shorter periods (< 60 min, i.e., < ~10 times the buoyancy period) and propagated more vertically than the waves observed by lidars (with typical periods of several hours and propagating more horizontally) [*Lu et al*., 2009, 2015b; *Chen et al*., 2016]. If the major AGW sources are the meteorological disturbances near the

Antarctic continent (e.g., a storm track at the latitude range of 50°S–60°S [*Trenberth*, 1991]), the AGW energy observed over Davis and Syowa in the mesosphere could be significantly larger than at the other two stations, McMurdo and Halley. On the other hand, inertia AGWs can propagate more horizontally and latitudinal difference could be smaller. We need more observational data and modeling to investigate this further.

3.2. Comparison With Blocking Diagram

In Figure 6 we show directionality of phase velocity spectra at Syowa and Davis and discuss the effect of background wind, derived from MERRA (the Modern Era Retrospective-Analysis for Research and Application) and MF radar observations [*Tsutsumi et al*., 2001]. MERRA is a reanalysis data composed of 288 × 144 grids with 1.25° longitude and 1.25° latitude resolution, 42 pressure levels (about 2 km interval above 20 km altitude), and a temporal resolution of 3 h [*Rienecker et al*., 2011]. MF radars at both stations have the same height resolution of 2 km. We selected these two stations because of the availability of MF radar winds. A blocking diagram described in *Taylor et al*. [1993] shows a phase velocity distribution of AGWs incapable of reaching airglow altitude due to background wind filtering. We derived blocking diagrams from the wind profiles of MERRA (altitude of 0–64 km) and the MF radar observations (altitude of 70–90 km at Syowa and 70–86 km at Davis) by linearly interpolating gaps between the altitude of MERRA and MF radars.

Figure 6a shows a phase velocity spectrum at Syowa at 18:38–21:48 UT on 3 May 2013. A peak of the spectrum was for 10–30 m/s and primarily in the northward direction. In comparison, power in the eastward and northeastward directions was rather small. Figure 6b plots combined wind profiles using 18:00 UT data from MERRA and the Syowa MF radar between 18:00 and 19:00 UT on the same day. The zonal wind was positive (i.e., eastward) between the ground and 90 km altitude with a strong eastward peak at 55 km with a magnitude of 90 m/s. The meridional wind was weakly negative (southward) and gradually increasing with altitude up to 80 km (~20 m/s). The corresponding wave blocking diagram is plotted in Figure 6c. A major part of the blocked area was in the eastward direction and agreed well with the observed wave spectra (Figure 6a) where the spectral power in the eastward direction was generally very weak.

Figures 6d–6e show a similar set of plots for data obtained 2 days later on 5 May 2013. The spectrum (Figure 6d) showed slightly different directionality with a more enhanced region in the northward-northeastward direction and lower power in the southeastward-eastward direction. A blocking diagram in Figure 6f shows a weaker blocked area in the northward-northeastward sector and stronger one in the southeastward-eastward sector, again consistent with the directionality shown in Figure 6d.

Figures 6g–6i display the results of a similar analysis for Davis on 21 April 2013. The spectrum observed at 21:40–00:27 UT (Figure 6g) exhibited strong enhancement in the wave activity in almost all directions except toward the north. Wind profiles from the MERRA and MF radar winds between 0 km and 85 km altitude were basically eastward, with weak meridional component, which was similar to Syowa. A resultant blocking diagram in Figure 6i suggests eastward propagating gravity waves should be significantly blocked. This is not consistent with the observed directionality shown in Figure 6g.

An example of the next day at Davis, 22 April, shown in Figures 6j–6l, indicates a very similar situation to Figures 6g–6i. Directionality was omnidirectional, but a wind-derived blocking diagram again showed only restricted vertical propagation for eastward propagating AGWs.

The lack of the eastward propagating AGWs over Syowa in Figures 6a and 6d can be explained by the fact that the AGWs were generated below the stratosphere and restricted to propagate vertically by the critical level filtering by the variable polar night jet. On the other hand, the directionalities in the phase velocity spectra over Davis in Figures 6g and 6j were not consistent with the blocking diagrams shown in Figures 6i and 6l. This suggests that the AGWs observed over Davis with the eastward propagation direction may have been generated at higher altitudes above which the critical level filtering by the polar night jet was not effective, although the relative location of Davis and the polar night jet is similar to that of Syowa and the polar night jet. This would also explain the more uniform directionality of the averaged wave spectrum at Davis as shown in Figure 4b and described in section 3.1. There are several studies suggesting AGW generation in the stratosphere based on lidar observations [e.g., *Lu et al*., 2015b]. However, these studies could not identify the altitude at which AGWs were generated. Our study successfully inferred an altitude of AGW generation by using the phase velocity distribution derived from the airglow imaging observation and the blocking diagram.

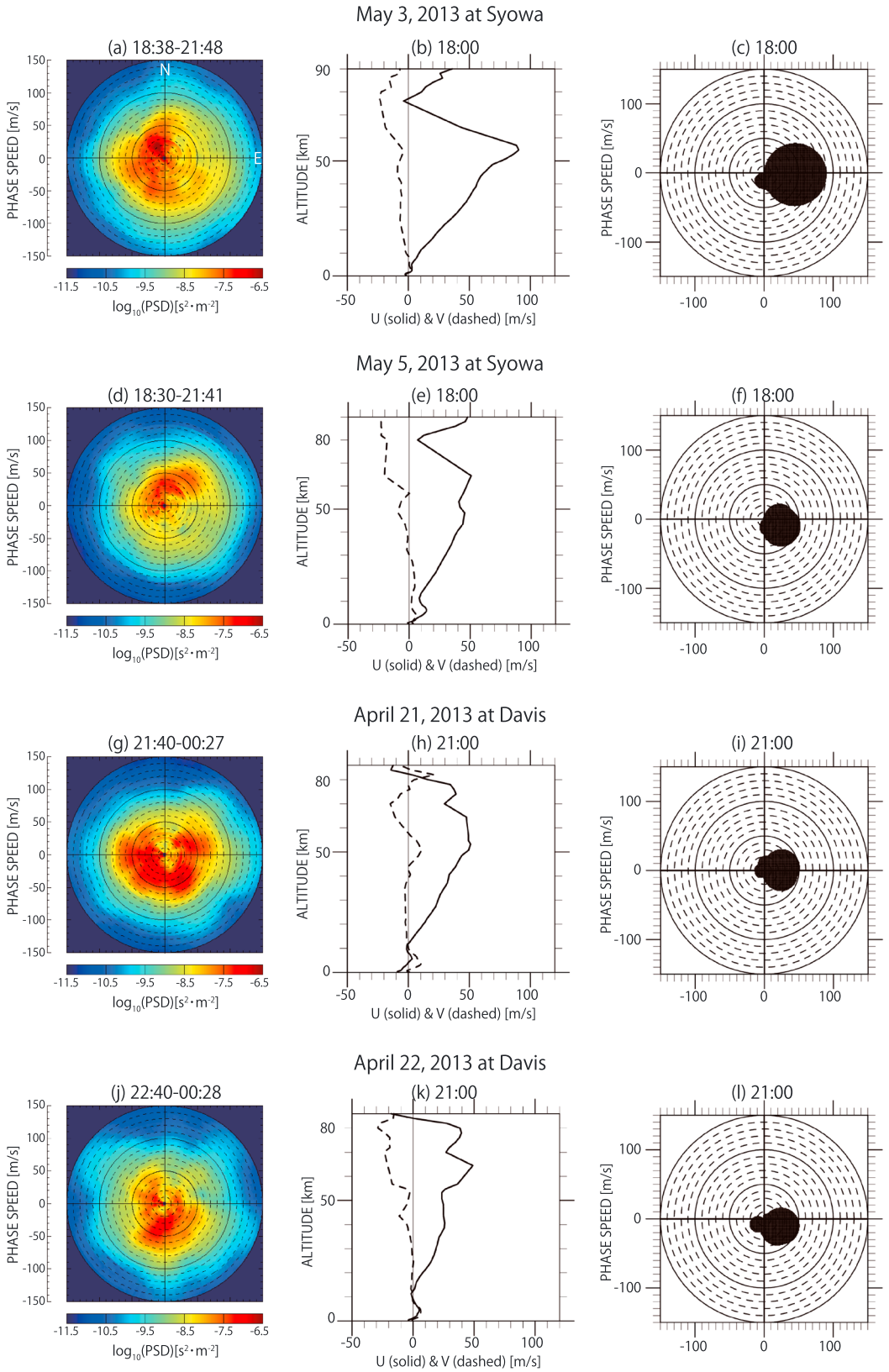

Figure 6. (a) Phase velocity spectra at 18:38–21:48 UT on 3 May 2013 at Syowa. (b) Zonal (solid) and meridional (dashed) wind velocity profiles at 18:00 UT derived from MERRA and MF radar. (c) Blocking diagram for the wind profiles shown in Figure 6b. (d–f) The same as Figures 6a–6c except for 5 May. (g–i) The case on 21 April 2013 at Davis. (j–l) For 22 April 2013 at Davis. Observation time is displayed at the top of each spectra.

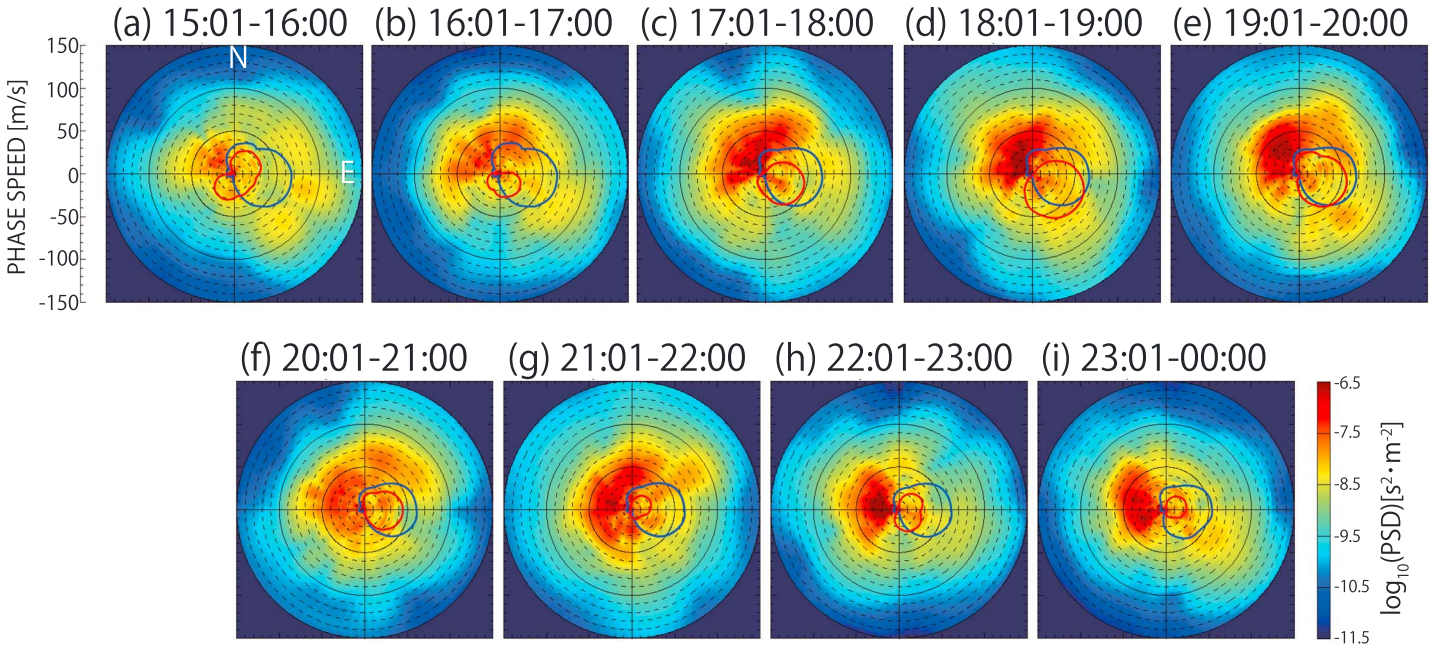

Figure 7. (a–i) Hourly average phase velocity spectra observed between 15:00 UT on 11 May and 00:00 UT on 12 May 2013 at Syowa. Blue and red circles indicate blocking diagram calculated using MERRA wind (0–64 km) and MF radar wind (70–90 km). Note that MERRA wind is provided every 3 h.

3.3. Temporal Variation on the Night of 11–12 May 2013

The airglow imaging technique has the advantage of almost continuous observations from a fixed observation site. Here we show analysis of nighttime variations of hourly mean phase velocity spectra and compare them with their corresponding blocking diagrams.

Figures 7a–7i show hourly mean phase velocity spectra for 9 h between 15:00 UT on 11 May and 00:00 UT on 12 May 2013 at Syowa Station.

A spectrum at 15:00–16:00 UT on 11 May 2013 at Syowa (Figure 7a) shows enhancement in the northwestward direction (270–350°) for phase speeds <60 m/s. A blocking diagram from MERRA (0–64 km, blue line) in Figure 7a shows that the eastward AGWs are blocked, whereas a blocked area from the MF radar (70–90 km, red line) lies between the northward, eastward, and southwestward directions. The observed direction of the enhancement in the wave spectrum is consistent with these combined blocking diagrams. It is also interesting that there was some enhancement in the northeastward, eastward, and southeastward directions just outside of the blocked area (plotted in blue) at the phase speeds around 60–120 m/s. An hour later, the region of enhancement of the spectrum in the northwestward expanded to the azimuth of 250–70° and with speeds up to 70 m/s, as shown in Figure 7b. For the next few hours, the enhancement grew stronger as plotted in Figures 7c–7e. A comparison of Figures 7a and 7d shows that the expansion of the northwestward enhancement to a larger region going from the northeast to the southwest is indeed consistent with the shrinking of the blocked area over the northeastward and the southwestward azimuth range. In Figures 7f and 7g the enhancement in the westward extended to the southward azimuths for phase speeds <50 m/s. After the enhancement of the same region in Figure 7g, at 22:00–23:00 UT, the enhancement in the northward and southward direction disappeared, and the dominant region remained only toward the westward (210–330°) direction for phase speeds <70 m/s as shown in Figure 7h.

In summary, the wave spectra exhibited enhanced regions mostly to the west with the weakest power toward the southeast, for phase speeds up to 70 m/s throughout the night. The weak region corresponded well to the blocked area as predicted by critical level filtering. The agreement between the variation of the directionality and the blocking diagram among Figures 7a, 7d, and 7g also suggests that critical level filtering by the background winds can affect significantly the directionality variation during the course of the night. However, there was no corresponding variation in the blocking diagrams in Figures 7g and 7h. This difference before and after 22:00 UT may have resulted from waves from a different source region,

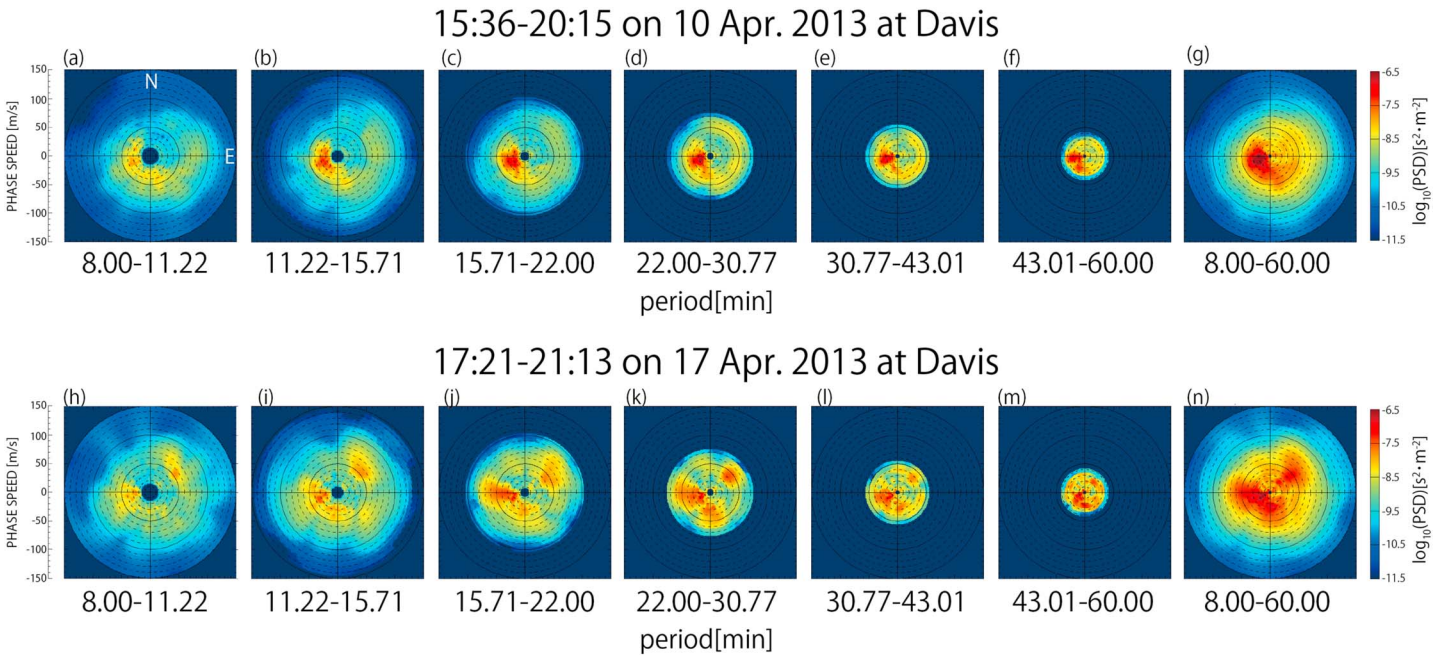

Figure 8. Phase velocity spectra for (a–f) six period bands and (g) all periods between 8 and 60 min observed at 15:36–20:15 UT on 10 April 2013 at Davis. (h–n) The same except for observation at 17:21–21:13 UT on 17 April 2013. Period bands are indicated at the bottom of the figures.

rather than the propagation conditions. Thus, the azimuthal extent and the temporal variation of the spectra cannot be explained only by critical level filtering by the background wind field, and source variations are also very important.

3.4. Wave Period Dependency of Directionality

In this section, we investigate difference in directionality between different observed wave periods, by dividing the phase velocity spectrum into six period bands. Period bands were selected to be 8–11, 11–15, 15–22, 22–30, 30–43, and 43–60 min, so that each period band has the same bandwidth normalized by the center period. Figures 8 and 9 show phase velocity spectra for these different period bands (a–f and h–m) and a phase velocity spectrum integrated for the entire 8–60 min band (g and n).

The first example was observed at 15:36–20:15 UT on 10 April 2013 at Davis. The spectrum in Figure 8g exhibited a spectral enhancement in the azimuth of 180–310° for phase speeds of 10–70 m/s, which can also be seen for all period bands in Figures 8a–8f. Enhancement in the southwestward direction (180–310°) with phase speeds up to 50 m/s became stronger for longer wave periods such as 15–60 min. This suggests that the AGWs corresponding to this enhancement had a broad spectrum in the wave period.

The second example (Figures 8h–8n) was observed at 17:21–21:13 UT on 17 April 2013 at Davis. The spectrum for the wave periods 8–60 min (Figure 8n) shows three enhanced regions: in the northeastward (20–90°, 20–90 m/s), southward (130–220°, 10–60 m/s), and westward (220–300°, 0–80 m/s) directions. The northeastward enhancement appeared for the 8–60 min band period (Figures 8h–8m), while the southward enhancement was clearly due to the 22–60 min band period (Figures 8k–8m). The westward enhancement appeared for the 8–30 min band period (Figures 8h–8k), but it was more southward for the 30–42 min band period (Figure 8l). This enhancement seems to have merged with the southward enhancement (Figure 8m) for the 43–60 min band period where only two enhanced regions could be recognized. Thus, the spectra on 17 April (Figures 8h–8n) appear to show different directionality depending on the wave period ranges, which was quite different from the spectra on 10 April (Figures 8a–8g).

The third example (Figures 9a–9g) was observed at 17:03–20:23 UT on 7 April 2013 at Syowa. In Figure 9f (43–60 min), there was an enhancement, which became stronger for longer periods. This suggested the existence of AGWs whose horizontal wavelength and period were out of the range for our analysis method.

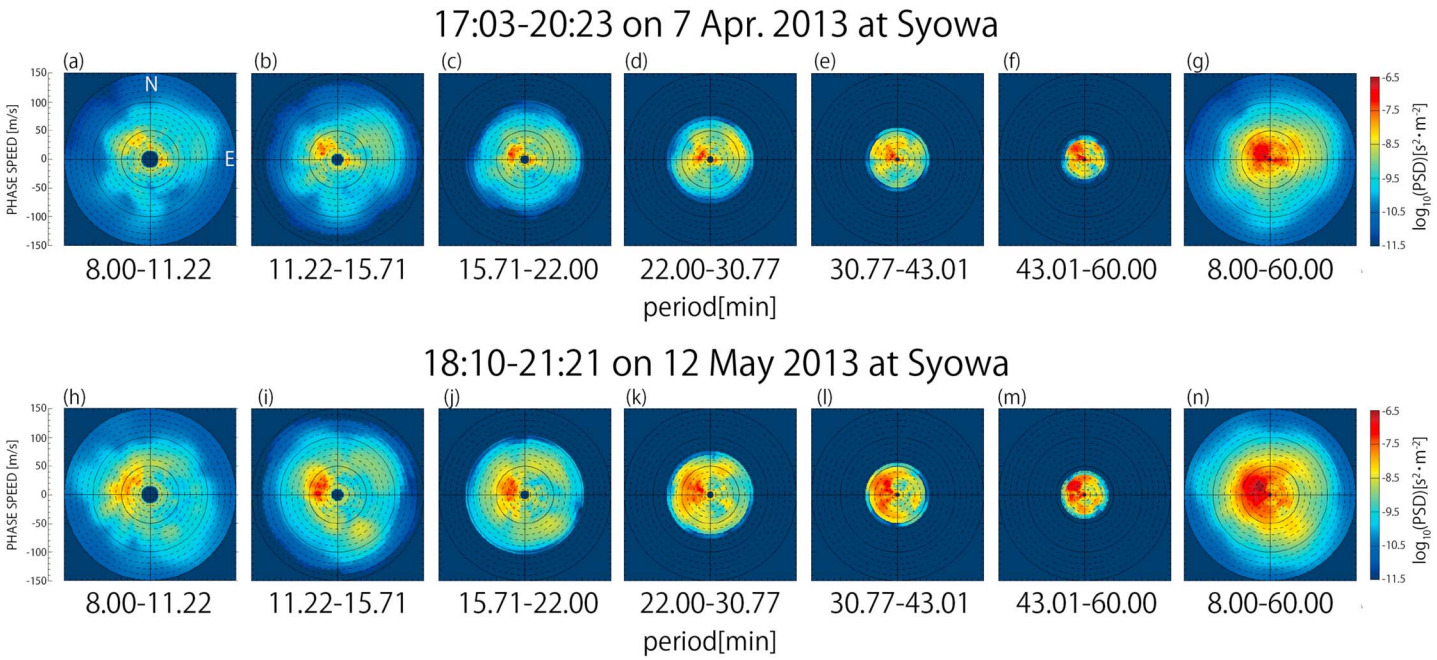

Figure 9. The same as Figure 8 except for observation at Syowa. Observation time was (a–g) 17:03–20:23 UT on 7 April 2013 at Syowa and (h–n) 18:10–21:21 UT on 12 May 2013.

The fourth example (Figures 9h–9n) was observed at 18:10–21:21 UT on 12 May 2013 at Syowa. The spectrum for the 8–11 min band (Figure 9h) exhibited an enhancement (240–340°) for phase speeds of 30–70 m/s, which became broader in azimuth for the 22–60 min band (Figures 9k–9m) and moved to lower phase speeds in the 8–30 min band (Figures 9h–9k).

Our results show that spectral power in Figures 9a–9g and 8h–8n was larger in the 22–60 min than the 8–22 min, although *Matsuda et al.* [2014] showed that AGW periods observed at Syowa in 2011 were mostly distributed in a period shorter than 20 min. It suggests that the spectral analysis method can be used to more precisely derive AGW propagation characteristics than the conventional event analysis method.

4. Conclusions

We have applied the new spectral analysis method to airglow data observed by several ANGWIN imagers sited around the Antarctic continent. The results from four stations, Syowa, Halley, Davis, and McMurdo, have been compared using the data obtained over an initial ~1.5 month period (from 6 April to 21 May 2013). The results obtained for the two consecutive nights at two different sites showed significant day-to-day and site-to-site differences. The averaged phase velocity distribution at the four stations showed the preferential propagation direction primarily toward the west at Syowa, at McMurdo, and at Halley. This could be caused by critical level filtering by the background wind field due to the strong polar night jet. However, the directionality at Davis was quite different and almost uniform. The blocking diagram at Syowa and Davis suggested that the eastward propagating AGW generated near the ground could not reach the airglow altitudes. The observed phase velocity spectra are consistent with this scenario at Syowa, but not at Davis. This result suggests that the AGWs over Davis may be generated above the stratosphere, where critical level filtering by the polar night jet is not effective. A possible source for these waves could be secondary wave generation, although more data are needed to reach a definitive conclusion. Detailed variations of the phase velocity spectra during the one night at hourly intervals at Syowa were compared with expectations from the blocking diagram. It was found that it is difficult to explain the hourly variations of the power spectrum by only considering the critical level filtering. The phase velocity spectrum with the different wave periods revealed the variation of directionality with the wave period as well as dominant wave period of each phase velocity spectral component. We showed that the spectral analysis technique allowed us to represent the directionality variation with the different period bands. This study is the first successful application of the new spectral analysis method developed by *Matsuda et al.* [2014] to the data observed by the ANGWIN network.

Acknowledgments
This work was supported by JSPS KAKENHI grant numbers JP24340121 and JP15H02137 and by JSPS Grant-in-Aid for JSPS Research Fellow grant number JP16J10875, and also subsidized by National Institute of Polar Research through Project Researches KP-2 and KP-301. Observation at Syowa station was carried out by JARE (Japan Antarctic Research Expedition) under the prioritized project AJ1. Operation of the Davis MF radar was supported by Australian Antarctica Science (AAS) project 4025. The Utah State University (USU) ANGWIN all-sky IR imagers at Halley, McMurdo, and Davis stations were funded and operated under NSF grants 1043356 and 1338666. The Halley imager is operated by British Antarctic Survey under a letter of agreement with USU while the Davis OH imager was operated under AAS projects 4025 and 4065. The authors are grateful for the efforts of the Davis wintering engineer. The MERRA data were obtained from http://disc.sci.gsfc.nasa.gov/. All the other data used in this study are available upon request. The contact points: the imager data at Syowa (nakamura.takuji@nipr.ac.jp) and at Davis, McMurdo, and Halley (mike.taylor@usu.edu). MF radar data for Syowa are available upon request (tsutsumi@nipr.ac.jp). MF radar data for Davis are available upon request (damian.murphy@aad.gov.au) or from the Australian Antarctic Data Centre at data.aad.gov.au.

References

Bageston, J. V., C. M. Wrasse, D. Gobbi, H. Takahashi, and P. B. Souza (2009), Observation of mesospheric gravity waves at Comandante Ferraz Antarctica Station (62°S), *Ann. Geophys.*, *27*(6), 2593–2598, doi:10.5194/angeo-27-2593-2009.

Chen, C., X. Chu, J. Zhao, B. R. Roberts, Z. Yu, W. Fong, X. Lu, and J. A. Smith (2016), Lidar observations of persistent inertia-gravity waves with periods of 3–10 h in the Antarctic middle and upper atmosphere at McMurdo, *J. Geophys. Res. Space Physics*, *121*, 1483–1502, doi:10.1002/2015JA022127.

Coble, M., G. C. Papen, and C. S. Gardner (1998), Computing two-dimensional unambiguous horizontal wavenumber spectra from OH airglow images, *IEEE Trans. Geosci. Remote Sens.*, *36*(2), 368–382, doi:10.1109/36.662723.

Ejiri, M. K., K. Shiokawa, T. Ogawa, K. Igarashi, T. Nakamura, and T. Tsuda (2003), Statistical study of short-period gravity waves in OH and OI nightglow images at two separated sites, *J. Geophys. Res.*, *108*(D21), 4679, doi:10.1029/2002JD002795.

Espy, P. J., G. O. L. Jones, G. R. Swenson, J. Tang, and M. J. Taylor (2004), Seasonal variations of the gravity wave momentum flux in the Antarctic mesosphere and lower thermosphere, *J. Geophys. Res.*, *109*, D23109, doi:10.1029/2003JD004446.

Espy, P. J., R. E. Hibbins, G. R. Swenson, J. Tang, M. J. Taylor, D. M. Riggin, and D. C. Fritts (2006), Regional variations of mesospheric gravity-wave momentum flux over Antarctica, *Ann. Geophys.*, *24*(1), 81–88, doi:10.5194/angeo-24-81-2006.

Fritts, D. C., and M. J. Alexander (2003), Gravity wave dynamics and effects in the middle atmosphere, *Rev. Geophys.*, *41*(1), 1003, doi:10.1029/2001RG000106.

Garcia, F., M. J. Taylor, and M. Kelley (1997), Two-dimensional spectral analysis of mesospheric airglow image data, *Appl. Opt.*, *36*(29), 7374–7385.

Gardner, C. S., K. Gulati, Y. Zhao, and G. Swenson (1999), Measuring gravity wave momentum fluxes with airglow imagers, *J. Geophys. Res.*, *104*(D10), 1903–1915.

Hapgood, M., and M. J. Taylor (1982), Analysis of airglow image data, *Ann. Geophys.*, *38*, 805–813.

Hecht, J. H., R. L. Walterscheid, M. P. Hickey, and S. J. Franke (2001), Climatology and modeling of quasi-monochromatic atmospheric gravity waves observed over Urbana Illinois, *J. Geophys. Res.*, *106*(D6), 5181–5195, doi:10.1029/2000JD900722.

Li, Z., A. Z. Liu, X. Lu, G. R. Swenson, and S. J. Franke (2011), Gravity wave characteristics from OH airglow imager over Maui, *J. Geophys. Res.*, *116*, D22115, doi:10.1029/2011JD015870.

Lindzen, R. S. (1981), Turbulence and stress owing to gravity wave and tidal breakdown, *J. Geophys. Res.*, *86*(C10), 9707–9714, doi:10.1029/JC086iC10p09707.

Lu, X., A. Z. Liu, G. R. Swenson, T. Li, T. Leblanc, and I. S. McDermid (2009), Gravity wave propagation and dissipation from the stratosphere to the lower thermosphere, *J. Geophys. Res.*, *114*, D11101, doi:10.1029/2008JD010112.

Lu, X., C. Chen, W. Huang, J. A. Smith, X. Chu, T. Yuan, P.-D. Pautet, M. J. Taylor, J. Gong, and C. Y. Cullens (2015a), A coordinated study of 1 h mesoscale gravity waves propagating from Logan to Boulder with CRRL Na Doppler lidars and temperature mapper, *J. Geophys. Res. Atmos.*, *120*, 10,006–10,021, doi:10.1002/2015JD023604.

Lu, X., X. Chu, W. Fong, C. Chen, Z. Yu, B. R. Roberts, and A. J. McDonald (2015b), Vertical evolution of potential energy density and vertical wave number spectrum of Antarctic gravity waves from 35 to 105 km at McMurdo (77.8°S, 166.7°E), *J. Geophys. Res. Atmos.*, *120*, 2719–2737, doi:10.1002/2014JD022751.

Matsuda, T. S., T. Nakamura, M. K. Ejiri, M. Tsutsumi, and K. Shiokawa (2014), New statistical analysis of the horizontal phase velocity distribution of gravity waves observed by airglow imaging, *J. Geophys. Res. Atmos.*, *119*, 9707–9718, doi:10.1002/2014JD021543.

Nakamura, T., A. Higashikawa, T. Tsuda, and Y. Matsushita (1999), Seasonal variations of gravity wave structures in OH airglow with a CCD imager at Shigaraki, *Earth Planets Space*, *51*(7), 897–906, doi:10.1186/BF03353248.

Nielsen, K., M. J. Taylor, R. E. Hibbins, and M. J. Jarvis (2009), Climatology of short-period mesospheric gravity waves over Halley, Antarctica (76°S, 27°W), *J. Atmos. Sol. Terr. Phys.*, *71*(8–9), 991–1000, doi:10.1016/j.jastp.2009.04.005.

Nielsen, K., M. J. Taylor, R. E. Hibbins, M. J. Jarvis, and J. M. Russell III (2012), On the nature of short-period mesospheric gravity wave propagation over Halley, Antarctica, *J. Geophys. Res.*, *117*, D05124, doi:10.1029/2011JD016261.

Rienecker, M. M., et al. (2011), MERRA: NASA's Modern-Era Retrospective Analysis for Research and Applications, *J. Clim.*, *24*(14), 3624–3648, doi:10.1175/JCLI-D-11-00015.1.

Suzuki, S., M. Tsutsumi, S. E. Palo, Y. Ebihara, M. Taguchi, and M. Ejiri (2011), Short-period gravity waves and ripples in the south pole mesosphere, *J. Geophys. Res.*, *116*, D19109, doi:10.1029/2011JD015882.

Taguchi, M., M. Ejiri, and K. Tomimatsu (2004), A new all-sky optics for aurora and airglow imaging, *Adv. Polar Upper Atmos. Res.*, *18*, 140–148.

Taylor, M. J., E. H. Ryan, T. F. Tuan, and R. Edwards (1993), Evidence of preferential directions for gravity wave propagation due to wind filtering in the middle atmosphere, *J. Geophys. Res.*, *98*(A4), 6047–6057, doi:10.1029/92JA02604.

Taylor, M. J., W. R. Pendleton Jr., S. Clark, H. Takahashi, D. Gobbi, and R. A. Goldberg (1997), Image measurements of short-period gravity waves at equatorial latitudes, *J. Geophys. Res.*, *102*(D22), 26,283–26,299, doi:10.1029/96JD03515.

Trenberth, K. (1991), Climate diagnostics from global analyses: Conservation of mass in ECMWF analyses, *J. Clim.*, *4*, 707–722, doi:10.1175/1520-0442(1991)004<0707:CDFGAC>2.0.CO;2.

Tsutsumi, M., T. Aso, and M. Ejiri (2001), Initial results of Syowa MF radar observations in Antarctica, *Adv. Polar Upper Atmos. Res*, *15*, 103–116.

Vincent, R. A. (1984), Gravity-wave motions in the mesosphere, *J. Atmos. Sol. Terr. Phys.*, *46*(2), 119–128, doi:10.1016/0021-9169(84)90137-5.

Walterscheid, R. L., J. H. Hecht, R. A. Vincent, I. M. Reid, J. Woithe, and M. P. Hickey (1999), Analysis and interpretation of airglow and radar observations of quasi-monochromatic gravity waves in the upper mesosphere and lower thermosphere over Adelaide, Australia (35°S, 138°E), *J. Atmos. Sol. Terr. Phys.*, *61*, 461–478, doi:10.1016/S1364-6826(99)00002-4.

Wrasse, C. M., et al. (2006), Mesospheric gravity waves observed near equatorial and low–middle latitude stations: Wave characteristics and reverse ray tracing results, *Ann. Geophys.*, *24*(12), 3229–3240, doi:10.5194/angeo-24-3229-2006.

Yamashita, C., X. Chu, H.-L. Liu, P. J. Espy, G. J. Nott, and W. Huang (2009), Stratospheric gravity wave characteristics and seasonal variations observed by lidar at the south pole and Rothera, Antarctica, *J. Geophys. Res.*, *114*, D12101, doi:10.1029/2008JD011472.